IET Communications

Research Article

IET Journals
The Institution of Engineering and Technology

Improved algorithm for joint detection and decoding on the joint sparse graph for CDMA systems

ISSN 1751-8628
Received on 5th June 2015
Revised on 7th October 2015
Accepted on 7th November 2015
doi: 10.1049/iet-com.2015.0506
www.ietdl.org

Lei Wen[1,2] ✉, *Jing Lei*[1], *Man Su*[2]

[1]*College of Electronic Science and Engineering, National University of Defence Technology, Changsha, People's Republic of China*
[2]*5G Innovation Centre, Institute for Communication Systems, University of Surrey, Guildford, United Kingdom*
✉ *E-mail: l.wen@surrey.ac.uk*

Abstract: Joint sparse graph for code division multiple access systems (JSG-CDMA) combines multiple accessing (low-density signature) and forward error correction (low-density parity check code) techniques, and it achieves satisfactory performance under overloaded conditions. In this study, the authors carry on the research on the joint detection and decoding for JSG-CDMA, and analyse the syndrome effect of message passing on the JSG by the extrinsic information transfer (EXIT) chart. An improved algorithm for joint detection and decoding on the JSG-CDMA receiver is proposed, and the convergence behaviour of the algorithm is analysed by EXIT chart. Simulation results show that improved algorithm enhance the system performance significantly with a marginal increase of the computational complexity.

1 Introduction

Code division multiple access (CDMA) is an important multiplexing technique where a number of users simultaneously and asynchronously access a channel by modulating and spread their information-bearing signals with pre-assigned signature sequences. CDMA has been used to support multimedia services in mobile radio communications, as it can cope with asynchronous nature of multimedia data traffic, to provide higher capacity over other access techniques such as time-division multiple access and frequency-division multiple access, and to combat the hostile channel frequency selectivity [1]. The capacity of a CDMA system is limited by inter-symbol-interference and multiple access interference (MAI) which results from channel noise and the imperfect correlation characteristic of spreading codes [2]. In uplink transmissions, when the number of user inevitably exceeds that of available chips, it is impossible to obtain the orthogonality of received signatures, consequently the system will be trapped into an overloaded condition where the MAI cannot be eliminated even if sophisticated multiuser detection (MUD) methods such as minimum mean-square error (MMSE) [3], serial interference canceller [4] and parallel interference canceller (PIC) [5] are adopted. To address this problem, it has been studied that the sequences meeting the Welch-bound-equality (WBE) can minimise the variance of the MAI [6], and the family of hierarchy of orthogonal subsets is another attempt to handle the overloaded conditions [7]. Moreover, a low-density signature (LDS) technique has been developed to enable CDMA systems to operate in overloaded multiuser environments with the performance that is close to a single user bound [8–10]. The LDS was modelled by a bipartite graph, and the belief propagation (BP) algorithm [11] is applied to perform MUD in the LDS-CDMA receiver.

Inspired by the similar structure of LDS and low density parity check (LDPC) code [12], we have proposed a joint sparse graph for CDMA systems (JSG-CDMA) which combines multiple accessing (LDS-CDMA) and forward error correcting (LDPC) techniques [13]. The JSG includes single graphs of LDS and LDPC codes, and BP algorithm is employed on the JSG to perform joint detection and decoding. According to [14], a turbo structured LDS-CDMA has also been studied in [13], where the soft information between MUD and channel decoding is iterated and exchanged through interleavers. Revealed by Wen and Su [13] and Koetter *et al.* [14], the performance of a turbo receiver is inferior to that of JSG-CDMA. It has been shown numerically and analytically that the JSG-CDMA can attain a satisfactory performance under overloaded conditions and outperforms conventional CDMA, LDS-CDMA as well as turbo structured LDS-CDMA [13]. However, it is still necessary to research the receiver technique of JSG-CDMA in detail, and improve the performance without dramatic increase of the computational complexity. This paper aims to further optimise overloaded JSG-CDMA systems, and the main contributions are listed as follows:

(i) The convergence behaviour of the joint detection and decoding in JSG-CDMA receiver is not ideal, consequently the system performance is not optimal. In the JSG, variable nodes play the bridge role to link chip nodes and parity check nodes, but the syndrome computing has not been drawn much attention. Due to the connected graph structure, we especially analyse the function of the syndrome computing in the joint detection and decoding, and introduce an extra parameter and a criterion for the chip nodes' updating. By doing so, more dependent information coming from variable nodes and parity check nodes is utilised by chip nodes, and the MAI can be eliminated more efficiently, as the updating of chip nodes is related to MUD directly. The convergence behaviour is analysed by extrinsic information transfer (EXIT) charts.
(ii) Considering the syndrome effect of the JSG, an improved algorithm for joint detection and decoding for JSG-CDMA is proposed. Compared with LDS-CDMA and standard JSG-CDMA, such improved algorithm can enhance the system performance significantly. The price of improved algorithm is an affordable increase of computational complexity from low to middle E_b/N_0 region.

The rest of this paper is organised as follows. Section 2 presents the transmitter diagram of JSG-CDMA system. In Section 3, the joint detection and decoding in the JSG-CDMA receiver is introduced. Syndrome effect on the message passing of the JSG is studied and analysed by the EXIT chart in Section 4, and simulation results are given in Section 5. Finally, Section 6 concludes the paper.

2 Transmitters of JSG-CDMA

The CMDA transmitters spread original data streams in the time domain using given spreading codes which are also named signatures, and the ability of suppressing MAI is determined by

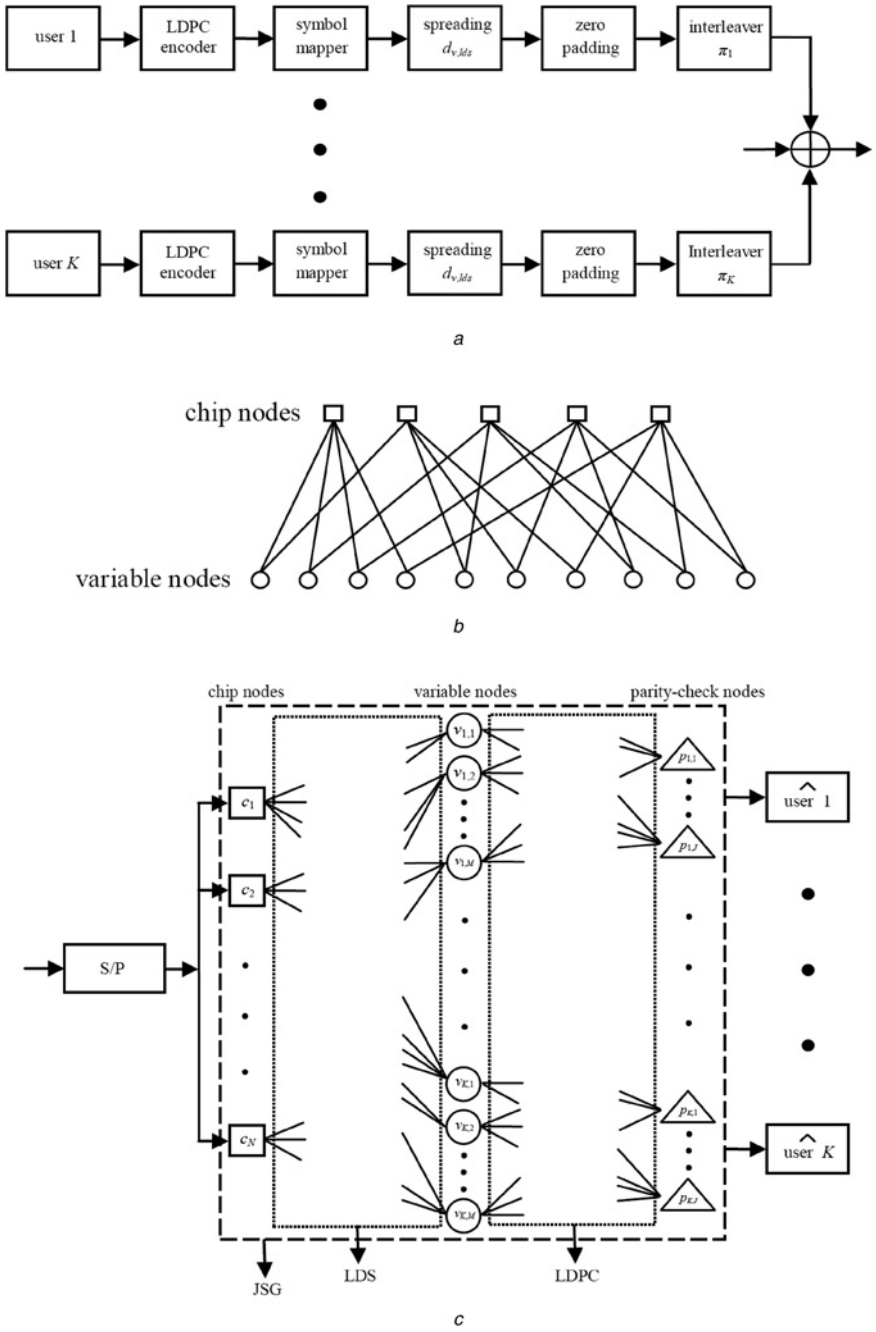

Fig. 1 *Block diagrams of the JSG-CDMA system*

a Transmitters of the JSG-CDMA
b Illustration of a LDS spreader
c Receivers of the JSG-CDMA

the cross-correlation characteristic of these spreading codes. Also, a frequency selective fading channel is characterised by the superimposition of several signals with different delays in the time domain. Therefore, the capability of distinguishing one data symbol from other data symbols in the composite received signal is determined by auto-correlation characteristic of the spreading codes. In conventional CDMA transmissions, the spreading code is optimised under certain criteria, e.g. good auto- and/or cross-correlation properties. However, it is impossible for the spreading codes to obtain the orthogonality under overload conditions, consequently the performance degrades dramatically as the desired (as well as the interferers') signal subspaces become rank-deficient. Meanwhile, conventional signatures naturally have high density, which means a lot of chips own non-zero values. Its drawback is that each user will be disturbed by the interference coming from all other users at the chip level.

Differing from conventional CDMA systems, JSG-CDMA transmitters spread their data on limited chips, and the block diagrams are shown in Fig. 1*a*. Consider the uplink communications with K users and processing gain of N. Each user has a data vector consisting of M modulated symbols, and a binary LDPC code with J parity check equations is used for forward error correcting. According to Fig. 1*a*, modulated streams including the user data is initially generated in a conventional manner, i.e. after LDPC encoding and symbol mapping, they are multiplied with a spreading signature (a sequence of N chips) to perform the spreading process. The differences between conventional CDMA and JSG-CDMA are listed as follows:

(i) In the JSG-CDMA spreading process, instead of optimising the N-chip sequences, the data symbols from the modulated data stream are spread over $d_{v,\mathrm{lds}}$ chips, where $d_{v,\mathrm{lds}}$ is much less than N. By doing so, each user will experience interference from only a

small number of other users' data symbols, and each chip is only used by a limited number of data symbols that may belong to different users. More explicitly, the number of symbols that are superimposed on each chip, which is referred to as $d_{c,\mathrm{lds}}$, is much less than the total number of modulated symbols, and the number of chips that are spread by each symbol, i.e. $d_{v,\mathrm{lds}}$, is much less than the total number of chips. In fact, the $d_{c,\mathrm{lds}}$ to $d_{v,\mathrm{lds}}$ ratio is related to the system loading.

(ii) The zero-padding is performed by adding $(N-d_{v,\mathrm{lds}})$ zeroes at the end of the signature for each user. As a result, the total processing gain of the system is kept to be N even when the effective chips for each data symbol to spread is much less than N. In other words, the generated sequences have a maximum of $d_{v,\mathrm{lds}}$ non-zero values and $(N-d_{v,\mathrm{lds}})$ zeroes (the term non-zero means there is an edge connecting a chip and a data symbol, while the term zero means there is no edge between the chip and the data symbol), and the resultant signature becomes very sparse. The zero-padding limits the amount of interference occurred on each user.

(iii) After the spreading and the zero-padding processes, a random interleaving pattern is applied to the zero-padded signature. Such interleaving process is designed to uniquely permutate chips for each user so that at each received chip there exist a contribution of, instead of all users, only a small number of users. Meanwhile, it determines edge connections between chips and data symbols, and changes the interference pattern being seen by each user. Hence, the interleavers define a spreading matrix that identifies the chips on which the users will spread their data at any given point in time.

A simple exemplary system with five chips and ten users is described in Fig. 1*b*, which schematically illustrates the sequence of operations carried out in Fig. 1*a*. The LDS can be represented by using a bipartite graph, where the chip nodes represent the chips and the variable nodes correspond to the symbols, for all symbols m and users from 1 to K. It can be seen that each symbol is spread over two chips, and each chip is spread by four symbols. Each user will experience interference from only a small number of other data symbols. One of the main advantages of the JSG-CDMA is its ability to support high loads while maintaining affordable receiver complexity and good performance. In the next section, we describe the joint detection and decoding in the receiver.

3 Joint detection and decoding in JSG-CDMA receivers

The receiver of JSG-CDMA is shown in Fig. 1*c*. It is significantly different from that of conventional CDMA, and there are three kinds of nodes in the figure: chip nodes c_n ($n \in [1, N]$), variable nodes $v_{k,m}$ ($k \in [1, K]$, $m \in [1, M]$) and parity check nodes $p_{k,j}$ ($k \in [1, K]$, $j \in [1, J]$), representing the nth chip, the mth data symbol and the jth parity check equation of the kth user, respectively. The iterative structure of the JSG can be clearly seen in the figure: a single sparse graph, as labelled by LDS in the left dash box, represents the LDS due to LDS-CDMA; the other single sparse graphs, as labelled by LDPC in the right dash box, represent the LDPC matrices due to LDPC codes. These two types of single sparse graphs belong to the techniques of multiple access and channel coding. Variable nodes (middle small circles) are used to connect the other two types of nodes (chip nodes and parity check nodes) through low density edges. Therefore, the receiver becomes a JSG which is labelled by JSG in the figure. As such, the LDS structure and LDPC code are perfectly linked together. Note that such receiver is different from turbo structured receivers, as there is no outer-inner turbo style iteration in Fig. 1*c*. On the basis of BP algorithm, MUD and channel decoding can be performed jointly on the whole sparse graph.

We assume that perfect channel state information is available at the receiver. Let the spreading signature for the kth user is $bfS_k = [s_{k,1}, \ldots, s_{k,M}] \in C^{N\times M}$, where C denotes complex field. Let $\boldsymbol{S} = [\boldsymbol{S}_1, \ldots, \boldsymbol{S}_K] \in C^{N\times M\times K}$ and $\boldsymbol{H} = [\boldsymbol{H}_1, \ldots, \boldsymbol{H}_K] \in C^{J\times M\times K}$ be the low density spreading signatures for CDMA and the LDPC matrices for LDPC code, respectively. We also define $\boldsymbol{T} = \mathrm{diag}(\boldsymbol{T}_1, \ldots, \boldsymbol{T}_K)$ as the transmit power gain of users and $\boldsymbol{G}_k = \mathrm{diag}(g_{k,1}, \ldots, g_{k,N})$ as the corresponding channel gain for the kth user. Moreover, $\psi_n = \{(k, m): s^n_{k,m} \neq 0\}$ and $\varepsilon_{k,m} = \{n: s^n_{k,m} \neq 0\}$ are the set of data symbols (which may belong to different users) that interfere on chip c_n and the set of chips that $v_{k,\,m}$ is spread on, respectively $\phi_j = \{(k, m): h^j_{k,m} \neq 0\}$ and $\omega_{k,m} = \{j: h^j_{k,m} \neq 0\}$ are the set of variable nodes that connect to parity check node $p_{k,\,j}$ and the set of parity check nodes that connect to $v_{k,m}$, respectively. In the receiver, received spreading sequences for the data symbol m of the kth user can be represented by $\boldsymbol{r}_{k,m} = \boldsymbol{T}_k \boldsymbol{G}_k s_{k,m}$. In particular, the received signature gain at the nth chip of the variable node $v_{k,m}$ is $r^n_{k,m} = \mathbf{T}_k g_{k,n} s^n_{k,m}$, thus the received signal corresponding to the nth chip can be expressed as

$$y_n = \sum_{k=1}^{K} \sum_{m=1}^{M} r^n_{k,m} v_{k,m} + z_n \tag{1}$$

where z_n is additive white Gaussian noise (AWGN) with variance σ^2_{A} and mean zero. Considering that in the JSG, the signature has a limited number of non-zero values, we can express the received signal at the nth chip as

$$y_n = \sum_{(k,m)\in\psi_n} r^n_{k,m} v_{k,m} + z_n \tag{2}$$

The log-likelihood ratio (LLR) exchanged between different kinds of nodes are denoted as follows: $L_{v_{k,m}\to c_n}$ and $L_{v_{k,m}\to p_{k,j}}$ are the LLR delivered from the variable node $v_{k,m}$ to the chip node c_n and the parity check node $p_{k,\,j}$, respectively; $L_{c_n\to v_{k,m}}$ and $L_{p_{k,j}\to v_{k,m}}$ are the LLR delivered from the chip node c_n and the parity check node $p_{k,j}$ to the variable node $v_{k,m}$, respectively. In this paper, we adopt a flooding schedule for the joint detection and decoding, i.e. all the message passing is processed in a parallel manner. The joint detection and decoding on the graphical model can be explained in the sequel.

(i) Variable nodes, parity check nodes and sparse edges between these two kinds of nodes constitute the parity check matrix of LDPC codes labelled by LDPC in Fig. 1*c*. In order to correct disturbed bits due to the channel noise, the soft message can be iteratively propagated along the edges for the decoding process. LLR of parity check nodes is calculated as [15]

$$L_{p_{k,j}\to v_{k,m}} = \varphi^{-1}\left(\sum_{(k',m')\in\phi_j\backslash(k,m)} \delta(L_{v_{k',m'}\to p_{k,j}})\right) \tag{3}$$

where $\phi_j\backslash(k, m)$ is the set of data symbols (excluding $v_{k,m}$) that connect to the parity check node $p_{k,j}$, and

$$\varphi(x) = \left(\mathrm{sign}(x),\ -\log\tanh\left(\frac{|x|}{2}\right)\right) \tag{4}$$

$$\varphi^{-1}(x) = (-1)^{\mathrm{sign}(x)}\left(-\log\tanh\left(\frac{|x|}{2}\right)\right) \tag{5}$$

where $\mathrm{sign}(\cdot)$ represents the sign of a variable, and such sub-graph in Fig. 1*c* belongs to the technique of forward error correcting.

(ii) Chip nodes, variable nodes and sparse edges between these two kinds of nodes constitute LDS of CDMA labelled by LDS in Fig. 1*c*. A chip node and a variable node are linked via an edge whenever such chip in the corresponding spreading code is non-zero. Obviously, the LDS is very similar to the Tanner graph of LDPC codes, and the soft message can also be iterated along the edges to perform MUD. Owing to the sparse structure, the MAI can be

IET Commun., 2016, Vol. 10, Iss. 3, pp. 336–345

effectively mitigated under overloaded conditions. LLR of chip nodes is updated as

$$L_{c_n \to v_{k,m}} = f(v_{k,m}|y_n, L_{v_{k',m'} \to c_n}, (k', m') \in \psi_n \backslash (k, m)) \quad (6)$$

where $\psi_n \backslash (k, m)$ is the set of data symbols (excluding $v_{k,m}$) that interfere on the chip c_n. In order to approximate the maximum a posteriori probability detector, the right hand side of (6) represents marginalisation function, which is based on (2), and can be written as

$$\begin{aligned} & f(v_{k,m}|y_n, L_{v_{k',m'} \to c_n}, (k', m') \in \psi_n \backslash (k, m)) \\ & \quad = \log\left(\sum p(y_n|\boldsymbol{v}) p_n(\boldsymbol{v}|v_{k,m})\right) \\ & \quad = \log\left(\sum p(y_n|\boldsymbol{v}) \prod_{(k',m') \in \psi_n \backslash (k,m)} p_n(v_{k',m'})\right) \end{aligned} \quad (7)$$

where $\boldsymbol{v}$ is the transmitted vector, the conditional probability density function $p(y_n|\boldsymbol{v})$ and a priori probability $p_n(v_{k',m'})$ are given as

$$p(y_n|\boldsymbol{v}) = \exp\left(-\frac{1}{2\sigma^2}||y_n - \boldsymbol{r}_{[n]}^{\mathrm{T}} \boldsymbol{v}_{[n]}||^2\right) \quad (8)$$

$$p_n(v_{k',m'}) = \exp\left(L_{v_{k',m'} \to c_n}\right) \quad (9)$$

where $\boldsymbol{v}_{[n]}$ and $\boldsymbol{r}_{[n]}$ denote the vectors containing the symbols transmitted by every user that spread its data on the nth chip and their corresponding effective received signature values, respectively. As can be seen from (7), based on the received chip y_n and a priori input information $p_n(v_{k',m'})$, extrinsic values are calculated for all the constituent bits involved in (2). Substituting (8) and (9) into (7), the message update becomes [10]

$$L_{c_n \to v_{k,m}} = \kappa_{n,k,m} \overset{*}{\max}_{\boldsymbol{v}_{[n]}} \left(\sum_{(k',m') \in \psi_n \backslash (k,m)} L_{v_{k',m'} \to c_n} - \frac{1}{2\sigma^2}||y_n - \boldsymbol{r}_{[n]}^{\mathrm{T}} \boldsymbol{v}_{[n]}||^2\right) \quad (10)$$

where $\kappa_{n,k,m}$ denotes the normalisation coefficient and

$$\overset{*}{\max}(a, b) = \max(a, b) + \ln\left(1 + \mathrm{e}^{-|a-b|}\right) \quad (11)$$

We can see that this sub-graph in Fig. 1*c* belongs to the technique of multiple accessing.

In the case of independent detection and decoding, variable node only gathers information from one type of node (chip node or parity check node). However, in Fig. 1*c*, variable node acts like a bridge that links chip nodes and parity check nodes in the receiver. As such, all the nodes and edges form a JSG labelled by JSG in the figure. The JSG combines multiple accessing and forward error correction techniques, and is different from turbo processing (in a turbo receiver, the decoder output is fed back to the detector input by interleavers, so the information of the detector and the decoder can be exchanged, and the system performance can be improved), as there is no outer-inner turbo style iteration in the JSG-CDMA receiver. On the basis of the JSG, the soft message can be exchanged for detection and decoding with low complexity, consequently the MAI and the channel noise can be eliminated effectively. For the variable node in Fig. 1*c*, the updating of $L_{v_{k,m} \to c_n}$ not only receives chip node information, but also utilises the information that comes from parity check nodes

$$L_{v_{k,m} \to c_n} = \sum_{n' \in \varepsilon_{k,m} \backslash n} L_{c_{n'} \to v_{k,m}} + \sum_{j \in \omega_{k,m}} L_{p_{k,j} \to v_{k,m}} \quad (12)$$

where $\varepsilon_{k,m} \backslash n$ is the set of chips (excluding c_{n}) that $v_{k,\,m}$ is spread on.

Similarly, updating of $L_{v_{k,m} \to p_{k,j}}$ also involves the information from both sides, i.e.

$$L_{v_{k,m} \to p_{k,j}} = \sum_{j' \in \omega_{k,m} \backslash j} L_{p_{k,j'} \to v_{k,m}} + \sum_{n \in \omega_{k,m}} L_{c_n \to v_{k,m}} \quad (13)$$

where $\omega_{k,m} \backslash j$ is the set of parity check nodes (excluding $p_{k,j}$) that connect to the variable node $v_{k,m}$.

A posterior probability of the transmitted symbol $v_{k,m}$ is calculated as

$$L_{v_{k,m}} = \sum_{n \in \varepsilon_{k,m}} L_{c_n \to v_{k,m}} + \sum_{j \in \omega_{k,m}} L_{p_{k,j} \to v_{k,m}} \quad (14)$$

where $L_{v_{k,m}}$ is the estimated LLR of the variable node $v_{k,m}$, and a hard decision is made

$$\hat{v}_{k,m} = \arg\max_{v_{k,m}} L_{v_{k,m}} \quad (15)$$

If syndrome $\boldsymbol{\hat{v}}\boldsymbol{H} = 0$ ($\hat{\boldsymbol{v}}$ is the estimated vector) or the maximum iteration number is reached, the process is terminated. Otherwise, the iteration goes on.

The syndrome computing is an inconspicuous process in the joint detection and decoding. Our following study reveals that such process is very important and sensitive to the JSG as it can yield extra diversity to the JSG-CDMA system.

4 EXIT chart analysis on the syndrome effect of the JSG

By combining the LDS and the LDPC code, the JSG provides a multiple accessing scheme that offers improved multiuser diversity in comparison to conventional CDMA and LDS-CDMA systems. On the JSG, BP algorithm influences both the convergence rate and the system performance. Due to the MAI and the channel noise, the propagated information may lead to inaccurate a posterior probability after several iterations, which means the unreliable message will affect the convergence of the message passing [16]. In order to improve the efficiency of the joint detection and decoding, we analyse the effect of syndrome computing on the JSG by EXIT charts.

4.1 Syndrome effect on message passing

According to Section 3, a JSG-CDMA receiver is designed to estimate the data symbols of different users from the received chips by applying BP algorithm to recover the data symbols based on the JSG combining the LDS spreading signature and LDPC parity check matrix. The syndrome computing is an easily neglectable process in the joint detection and decoding. According to the channel coding theory, syndromes in the LDPC decoding are only used to determine whether quit the current iteration [17, 18]. However, the JSG in Fig. 1*c* contains not only Tanner graph of LDPC codes but also sparse signatures of CDMA processing. Thus the syndrome computing is related to both LDPC decoding and MUD, and it is necessary to research how to utilise the information provided by syndromes.

A parity check node substantially plays the role of parity check equation in the JSG. Generally speaking, if all the syndromes of the parity check nodes equal to zeroes, the decoded-word is a valid codeword, and the process can be regarded as a successful decoding (excluding some extreme cases under the severe channel noise that a codeword may be decoded into another codeword). The JSG-CDMA receiver treats received signals due to other active users as stationary interference, while by applying BP algorithm, the receiver jointly detects and decodes those signals in order to mitigate the non-orthogonal properties of the received

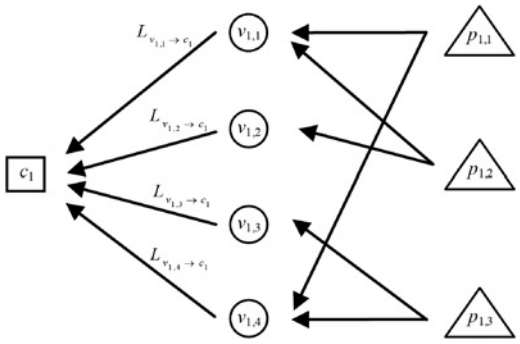

Fig. 2 *Example of message passing on a sub-graph in JSG-CDMA*

signals. As variable nodes connect both chip nodes and variable nodes, it is possible to utilise the extra information provided by the syndrome during the process of chip node updating. Fig. 2 shows an example of the message passing on a sub-graph which is extracted from the JSG of Fig. 1*c*. For instance, in a typical iteration, syndromes of parity check nodes $p_{1,1}$ and $p_{1,2}$ both equal to zero, but the syndrome of $p_{1,3}$ contains non-zero values. In the information theory, such result indicates that the information coming from $p_{1,1}$ and $p_{1,2}$ is highly dependable. Due to the fact that $v_{1,1}$ and $v_{1,2}$ are linked to $p_{1,1}$ and $p_{1,2}$ via corresponding edges, thus when chip node c_1 updates, we can magnify $L_{v_{1,1}\to c_1}$ and $L_{v_{1,2}\to c_1}$ by multiplying a coefficient α, where $\alpha \geq 1$ and can be adapted to the channel condition. It is noteworthy that although $v_{1,4}$ is linked to $p_{1,1}$, $L_{v_{1,4}\to c_1}$ cannot be magnified. This is due to that $v_{1,4}$ is also connected to $p_{1,3}$ whose syndrome has non-zero elements, consequently the information coming from $v_{1,4}$ is not very dependable. Therefore, $L_{v_{1,3}\to c_1}$ and $L_{v_{1,4}\to c_1}$ are handled in the conventional manner. As explained above, (10) can be reformed as (see (16)) where $\text{syn}_{\omega_{k,m}} \neq 0$ and $\text{syn}_{\omega_{k,m}} = 0$ represent parity check nodes whose syndromes whether equal to all-zeroes.

Comparing with standard algorithm, we hereinafter refer the joint detection and decoding that takes account of the syndrome effect as an improved algorithm. The extra information coming from the syndrome can accelerate the convergence rate of BP algorithm and reduce iteration numbers, which will be further analysed by the EXIT chart.

4.2 EXIT chart analysis

The EXIT chart is an effective tool to analyse iterative systems [19, 20]. For convenience, we define the following notations: CND – chip node detector, VNDD – variable node detector and decoder, PND – parity check node decoder, $I_{\text{A,VNDD}}$ – the average mutual information between the bits on the VNDD edges and the a priori LLR, $I_{\text{E,VNDD}}$ – the average mutual information between the bits on the VNDD edges and the extrinsic LLR, $I_{\text{A,CND\&PND}}$ – the average mutual information between the bits on the CND&PND edges and the a priori LLR, $I_{\text{E,CND\&PND}}$ – the average mutual information between the bits on the CND&PND edges and the extrinsic LLR. A priori LLR can be calculated by

$$A = \mu_A x + z_n \tag{17}$$

where z_n is AWGN with variance σ_{A}^2 and mean zero; $x \in \pm 1$ is the bits on the graph edge. Furthermore

$$\mu_A = \frac{\sigma_{\text{A}}^2}{2} \tag{18}$$

The mutual information $I_{\text{A,VNDD}} = \text{I}(X;A)$ can be calculated by

$$\begin{aligned} I_{\text{A,VNDD}}(\sigma_{\text{A}}) &= \\ &\frac{1}{2}\sum_{x=-1,1}\int_{-\infty}^{+\infty} p_A(\beta|X=x)\log_2\frac{2p_A(\beta|X=x)}{p_A(\beta|X=-1)+p_A(\beta|X=1)}\,\text{d}\beta \\ &= 1-\int_{-\infty}^{+\infty}\frac{\text{e}^{-((\beta-\sigma_{\text{A}}^2/2)^2/2\sigma_{\text{A}}^2)}}{\sqrt{2\pi}\sigma_{\text{A}}}\log_2(1+\text{e}^{-\beta})\,\text{d}\beta \end{aligned} \tag{19}$$

For abbreviation we define

$$B(\sigma) := I_{\text{A,VNDD}}(\sigma_{\text{A}} = \sigma) \tag{20}$$

with

$$\lim_{\sigma\to 0} B(\sigma) = 0 \tag{21}$$

$$\lim_{\sigma\to \infty} B(\sigma) = 1 \tag{22}$$

where $\sigma \geq 0$. The EXIT function of a variable node can be expressed as

$$\begin{aligned} &I_{\text{E,VNDD}}(I_{\text{A,VNDD}}, d_{v,\text{lds}}, d_{v,\text{ldpc}}) = \\ &\qquad B\left(\sqrt{(d_{v,\text{lds}}+d_{v,\text{ldpc}}-1)(B^{-1}(I_{\text{A,VNDD}}))^2}\right) \end{aligned} \tag{23}$$

As shown in (3) and (16), a parity check node only has messages coming from neighboured variable nodes, while a chip node has incoming messages from the connected variable nodes and the channel. We model $L_{v_{k,m}\to p_{k,j}}$ and $L_{v_{k,m}\to c_n}$ as the output of the channel that the input is the corresponding transmitted bit, and then calculate the mutual information of the output with regards to the actual value on the edges. Due to the complexity of the calculation in parity check nodes and chip nodes, their EXIT curves are computed by simulations over channels. The probability density function for extrinsic information is determined by Monte Carlo simulation with histogram measurements, the mutual information between the extrinsic information and the bits on the edges, is subsequently calculated. For the following investigations, the system parameters are listed as follows: the user number is 240, the chip number is 120, the system loading is 200%, a half rate quaci-cyclic LDPC code is adopted, $d_{v,\text{lds}} = 3$, $d_{c,\text{lds}} = 6$, $d_{v,\text{ldpc}} = 3$ ($d_{v,\text{ldpc}}$ is the number of parity check nodes connected to each variable node in the JSG), $d_{p,\text{ldpc}} = 6$ ($d_{p,\text{ldpc}}$ is the number of variable nodes connected to each parity check node in the JSG), the channel model is Rayleigh fading channel. Fig. 3 shows the EXIT chart analysis of the JSG at different E_b/N_0. Throughout the simulations, the number of experiments run is 100,000 to ensure fair comparisons. According to the results, we can summarise:

(i) As $d_{v,\text{lds}} = 3$ and $d_{v,\text{ldpc}} = 3$, according to (23), the curves of VNDD are the same for the case of 6 dB and 12 dB.
(ii) For standard and improved algorithms, due to different E_b/N_0, the average level of CND&PND curves at 6 dB is lower than that at 12 dB. For example, in the beginning of the joint detection and decoding ($I_{\text{A, CND\&PND}}$ & $I_{\text{E,VNDD}} = 0$), $I_{\text{E,CND\&PND}}$ & $I_{\text{A,VNDD}}$ is approximately 0.095 at 6 dB, which is notably lower than that of 0.165 at 12 dB. At the end of the processing (intersection point of VNDD and CND&PND), the intersection point at 6 dB is much lower than that at 12 dB. In the EXIT chart, a higher intersection

$$L_{c_n\to v_{k,m}} = \kappa_{n,k,m}\max_{\boldsymbol{v}_{[n]}}{}^{*}\left(\sum_{(k',m')\in\psi_n\backslash(k,m)\ \&\ \text{syn}_{\omega_{k,m}}\neq 0} L_{v_{k',m'}\to c_n} + \sum_{(k',m')\in\psi_n\backslash(k,m)\ \&\ \text{syn}_{\omega_{k,m}}=0} \alpha L_{v_{k',m'}\to c_n} - \frac{1}{2\sigma^2}||y_n - \boldsymbol{r}_{[n]}^{\text{T}}\boldsymbol{v}_{[n]}||^2\right) \tag{16}$$

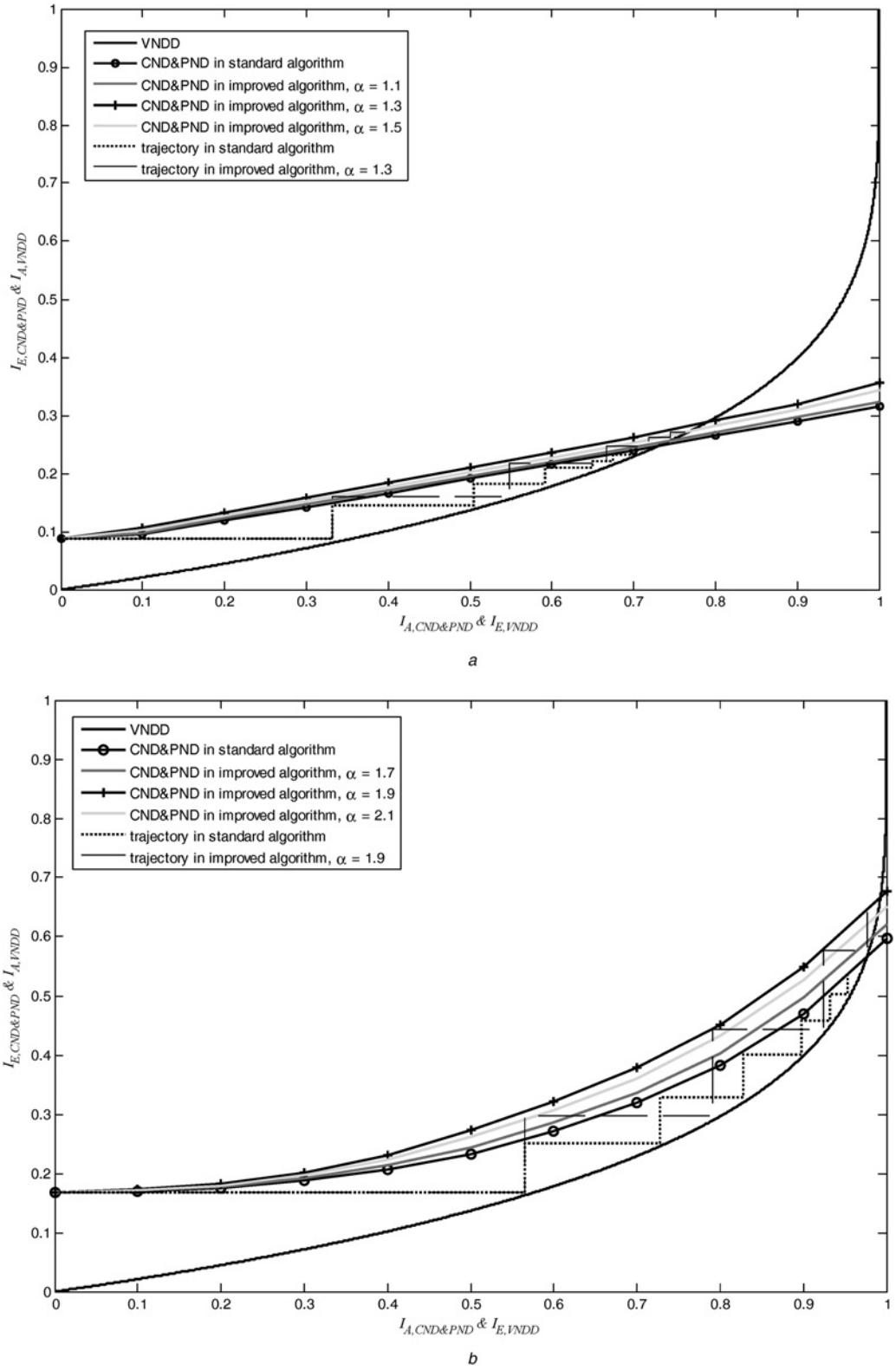

Fig. 3 *EXIT chart analysis of the joint sparse graph*

a $E_b/N_0 = 6$ dB
b $E_b/N_0 = 12$ dB

point means more extrinsic information can be utilised and a better performance can be achieved. Therefore, the EXIT chart in Fig. 3 verifies that the JSG-CDMA receiver will obtain a lower bit error rate (BER) at the higher E_b/N_0.

(iii) At different E_b/N_0, the CND&PND curves of improved algorithm with different α are always higher than that of standard algorithm, except in the beginning of the joint detection and decoding. There is no difference of a priori information during the first iteration for these two algorithms. However, as the iteration increases, improved algorithm lifts the CND&PND curve effectively, which means more reliable information is extracted and iterated by the syndrome effect process in (16). Moreover, the intersection point of VNDD and CND&PND in improved algorithm is always higher than that of standard algorithm. Such

phenomenon indicates that a better performance can be achieved by adopting improved algorithm.
(iv) As for the value of α in improved algorithm, we analyse it in the EXIT chart in detail. In Fig. 3*a*, when $\alpha = 1.1$, the CND&PND curve and the intersection point in improved algorithm are slightly higher than that of standard algorithm, which means a marginal improvement can be obtained by improved algorithm. When $\alpha = 1.3$, for the CND&PND curves, the gap between the standard and improved algorithms is very apparent and almost maximised. However, when α keeps on increasing, e.g. $\alpha = 1.5$, the CND&PND curve descends rather than continues to lift. In the low E_b/N_0 region, there is severe channel noise, thus the probability of decoding a codeword into another codeword is relatively high. In that extreme case, the message coming from the variable nodes is undependable even if their syndromes equal to zeroes. Therefore, the performance cannot be immensely improved with increasing value of α. There is a tradeoff between the syndrome effect and false decoding probability. According to the EXIT chart analysis, we suggest setting $1.2 < \alpha < 1.4$ in the low E_b/N_0 region. As for the relatively high E_b/N_0 region, the effect of α in the EXIT chart is also analysed in Fig. 3*b*. It can be seen that 1.7 valued α lifts the CND&PND curve and the intersection point, while 1.9 valued α shows more distinct improvement. Similarly, it is impossible to unlimitedly promote the CND&PND curve with increasing value of α. For example, compared with 1.9 valued α, 2.1 valued α leads to even lower CND&PND level. We suggest setting $1.8 < \alpha < 2.0$ in the middle to high E_b/N_0 region. Due to the assumption that perfect channel state information is available at the receiver, the JSG can choose proper value of α according to the E_b/N_0 condition and other parameters such as overloading condition.
(v) Trajectories of the joint detection and decoding are plotted in the figure. At $E_b/N_0 = 6$ dB, six iterations are needed to get to the intersection point for both algorithms. At $E_b/N_0 = 12$ dB, there are six iterations in the EXIT chart for standard algorithm. As for improved algorithm with $\alpha = 1.9$ at 12 dB, the iteration number is decreased to four.

As explained above, the syndrome effect results in an improved algorithm that is more robust to interference on different users' data symbols, by increasing the system diversity. When executing the joint detection and decoding at JSG-CDMA receiver, the more syndromes that are calculated, the more dependable information that can be utilised as the number of iteration increases.

5 Simulation results

In this section, the JSG-CDMA receiver utilising the different algorithms described before is evaluated over a Rayleigh fading channels. The chip number is 120, and a binary phase shift keying (BPSK) mapping is performed. In addition, a half rate quaci-cyclic LDPC code is adopted for all the investigated systems [21]. For comparisons, CDMA and LDS-CDMA systems are also simulated. For CDMA system, WBE that minimises the variance of the MAI, is used for the spreading sequences, and an MMSE-based PIC detector is used for MUD [3]. For LDS-CDMA, the effective spreading factor is 3 and an iterative detector is adopted [10]. The maximum number of iterations are limited to seven for both LDS-CDMA and JSG-CDMA receivers.

5.1 Comparison between different systems

Fig. 4*a* shows the performance comparisons between different schemes with 200 and 300% system loadings. According to the figure, we can summarise as follows:

(i) For each system, the performance of 300% loading is inferior to that of 200% loading. This is related to the fact that the higher loading is evaluated, the severer MAI is encountered.
(ii) Under both 200 and 300% loadings, the conventional CDMA system with an MMSE-PIC detector fails to achieve a satisfactory performance. Such result indicates that conventional CDMA systems cannot work well in high overloading conditions.
(iii) The low density structured CDMA systems, including LDS-CDMA and JSG-CDMA, exhibit much better performance than that of conventional CDMA. Their performance improvement is mainly due to the capability of the LDS to exploit time domain diversity and avoid a strong interference to corrupt all the data symbols.
(iv) The JSG-CDMA receivers, regardless of standard or improved algorithm is utilised, are superior to the LDS-CDMA receiver. Take BER of 10^{-3} as an example, under 200% system loading, the JSG-CDMA can attain ~2–2.3 dB gain over the LDS-CDMA, while under 300% system loading, the improvement is about 2.1–2.4 dB. Hence, the JSG of JSG-CDMA outperforms the single graph of LDS-CDMA.
(v) For the JSG-CDMA receiver, when $E_b/N_0 < 10$ dB, the difference between standard and improved algorithms is marginal, which can be explained by observing the signal constellation at each chip and the dominating effect of noise at the low E_b/N_0 region. In the middle to high E_b/N_0 region, the advantage of improved algorithm is shown clearly. At a BER of 10^{-3}, compared with standard algorithm in 200 and 300% system loadings, improved algorithm can profit about 0.5 dB and 0.6 dB gains. As explained in Section 4, the iterative processing that takes account of the syndrome effect increases the ability of eliminating MAI and channel noise at the receiver side. Therefore, improved algorithm can enhance the system performance significantly.

5.2 Comparisons at different iterations for JSG-CDMA

To testify the convergence rate of different algorithms, Fig. 4*b* shows the performance comparison of 200% loaded JSG-CDMA at each iteration for different E_b/N_0 values. According to the figure, in the first iteration, the two algorithms always start at the same point since the syndrome can only be calculated after the first iteration. As the iteration increase, the BER drops dramatically. It can be seen that improved algorithm notably accelerates the downward tendency of the curves, especially at $E_b/N_0 = 12$ dB. Thus compared with standard algorithm, improved algorithm has faster convergence rate and better performance. Although at $E_b/N_0 = 6$ dB, the iteration numbers are the same for both algorithms, i.e. six iterations, but improved algorithm still can accelerate the convergence rate and enhance the system performance. More importantly, in the middle to high E_b/N_0 region, improved algorithm can decrease the iteration number significantly. For example, at $E_b/N_0 = 12$ dB, six iterations are required for standard algorithm to reach its convergence point, which means that the BER curve almost stop falling down after six iterations. By contrast, when improved algorithm is employed, the JSG-CDMA receiver only needs four iterations to get the convergence point. As a result, the iteration number and the transmission delay can both be optimised by improved algorithm. It is worth noting that the convergence behaviour and trajectory predicted by EXIT chart analysis in Fig. 3 are verified by the BER result in Fig. 4*b*. Hence, the syndrome effect is a very important factor for the successful use of BP in the JSG-CDMA receiver, as it not only improves the system performance, but also optimises the convergence rate.

5.3 Individual users' behaviour

The performance of the best user and the worst user in 200% loaded JSG-CDMA is shown in Fig. 5, including the cases of standard and improved algorithms on the receiver side. The figure illustrates that some users have poor performance than the others, meaning that the JSG does not give equal multiuser efficiency or in other words it does not result in the same performance for all the users. However, the performance gap between the best user and the worst user in improved algorithm is slightly smaller than that of standard algorithm, indicating that a fairer and a more uniform user experience can be achieved by improved algorithm.

IET Commun., 2016, Vol. 10, Iss. 3, pp. 336–345

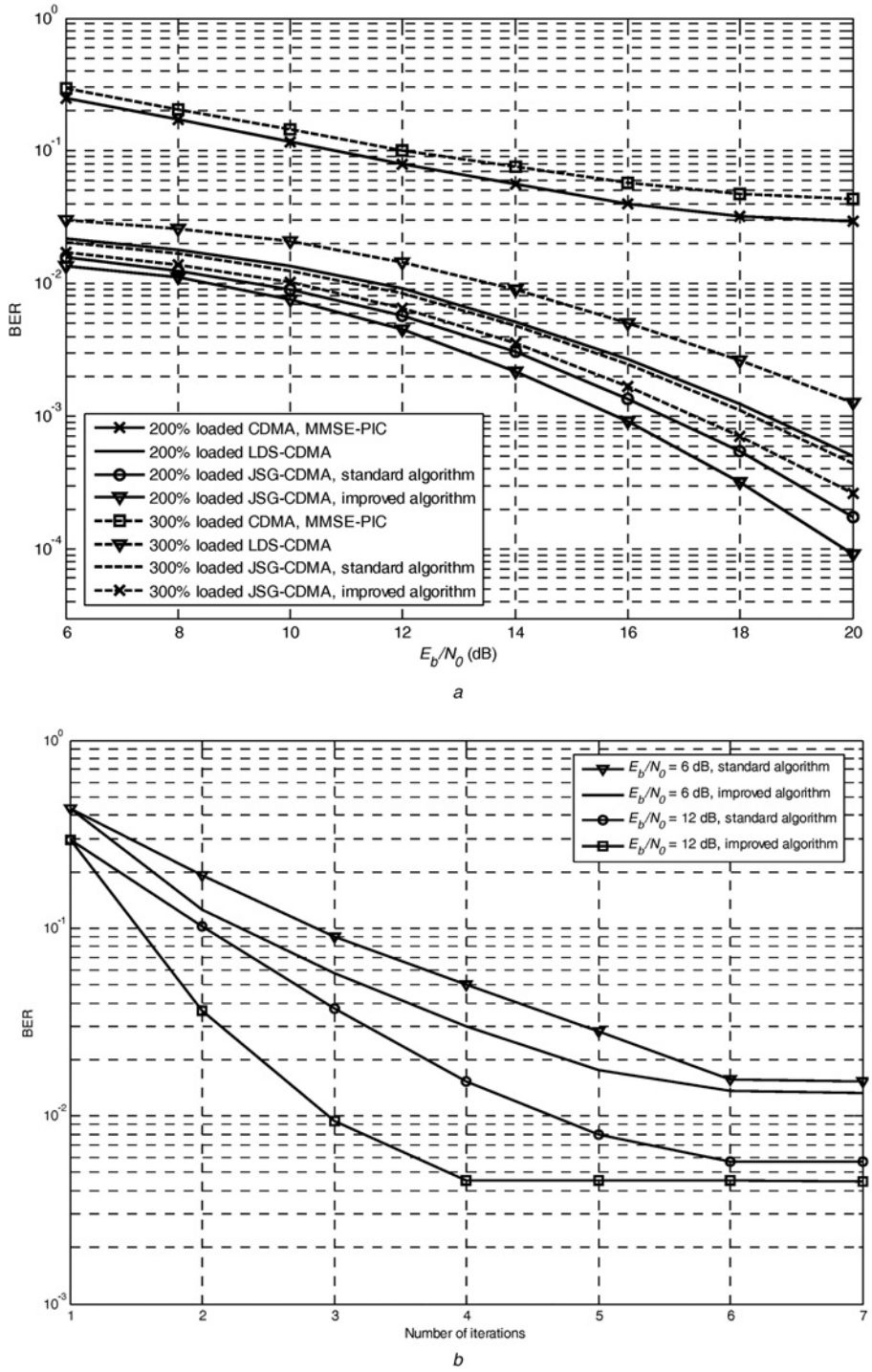

Fig. 4 *Performance comparisons*

a Comparison between different systems
b Comparison at different iterations for JSG-CDMA

5.4 Computational complexity

In this subsection, we compare the computational complexity between standard and improved algorithms. As can be seen from (16), in improved algorithm extra operations, which indicate if the variable node belongs to the zero-valued syndrome, are required. Meanwhile, the multiplication of the coefficient α is another extra operation to the receiver. Consequently, in a specific iteration, the cost of improved algorithm is higher than that of standard algorithm. However, according to the EXIT chart analysis and the BER results, in the middle to high E_b/N_0 region, the iteration number can be reduced by the use of improved algorithm. The above two factors should be considered. For a fair comparison, we express the complexity of the joint detection and decoding in terms of equivalent additions. The basic operations performed by BP algorithm include addition (ADD), subtraction (SUB), multiplication by ±1 (MUL), division by 2 (DIV), comparison (CP) and $max(x; y)$ (MAX). The ADD, SUB, MUL, DIV and CP operations correspond to one equivalent addition. Also, the MAX operation corresponds to two equivalent additions, since it first uses a CP operation to compare the two input values and then stores the result in a register [22]. Fig. 6 shows the numbers of equivalent addition operations for the joint detection and decoding in 200% loaded JSG-CDMA. It can be seen that for

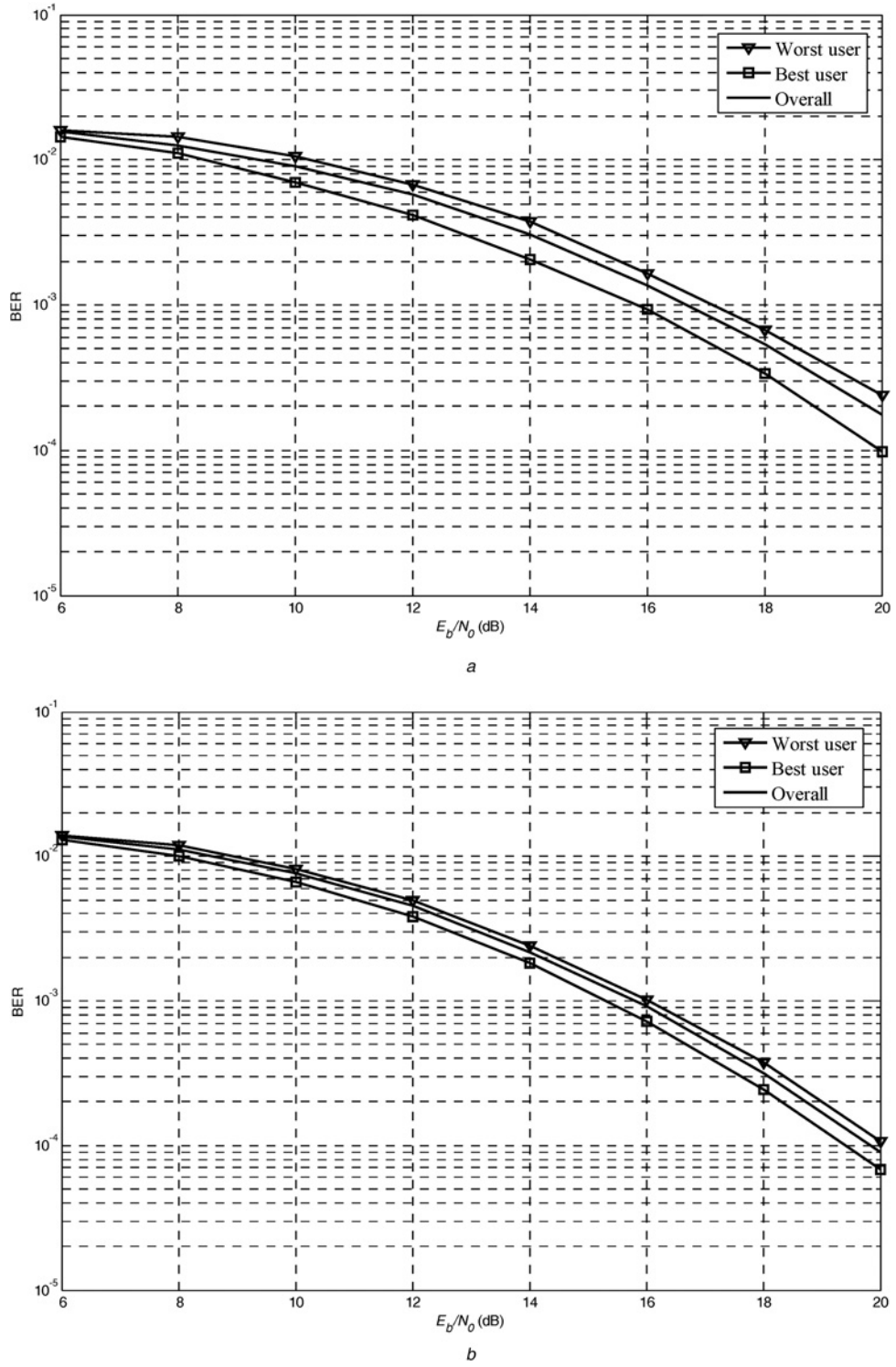

Fig. 5 *Performance of different users in JSG-CDMA*

a Standard algorithm
b Improved algorithm

each algorithm, the equivalent additions drop rapidly as the E_b/N_0 increases, which is related to the reduction of iterations when E_b/N_0 increases. Moreover, the figure also reveals that in the low E_b/N_0 region, the complexity of improved algorithm is distinctly higher than that of standard algorithm. In the middle E_b/N_0 region, the numbers of equivalent additions are almost the same for the two algorithms. Note that in the high E_b/N_0 region, the complexity of improved algorithm is even lower than that of standard algorithm. Such phenomenon can be attributed to the difference of the iteration number between the two algorithms. More explicitly, when E_b/N_0 is relatively high, improved algorithm can accelerate the convergence rate and reduce the iteration number, thus the equivalent additions are less than that of standard algorithm. Therefore, in the high E_b/N_0 region, improved algorithm not only improves the system performance, but also reduces the receiver complexity. On average, improved algorithm requires higher computational complexity than standard algorithm.

IET Commun., 2016, Vol. 10, Iss. 3, pp. 336–345

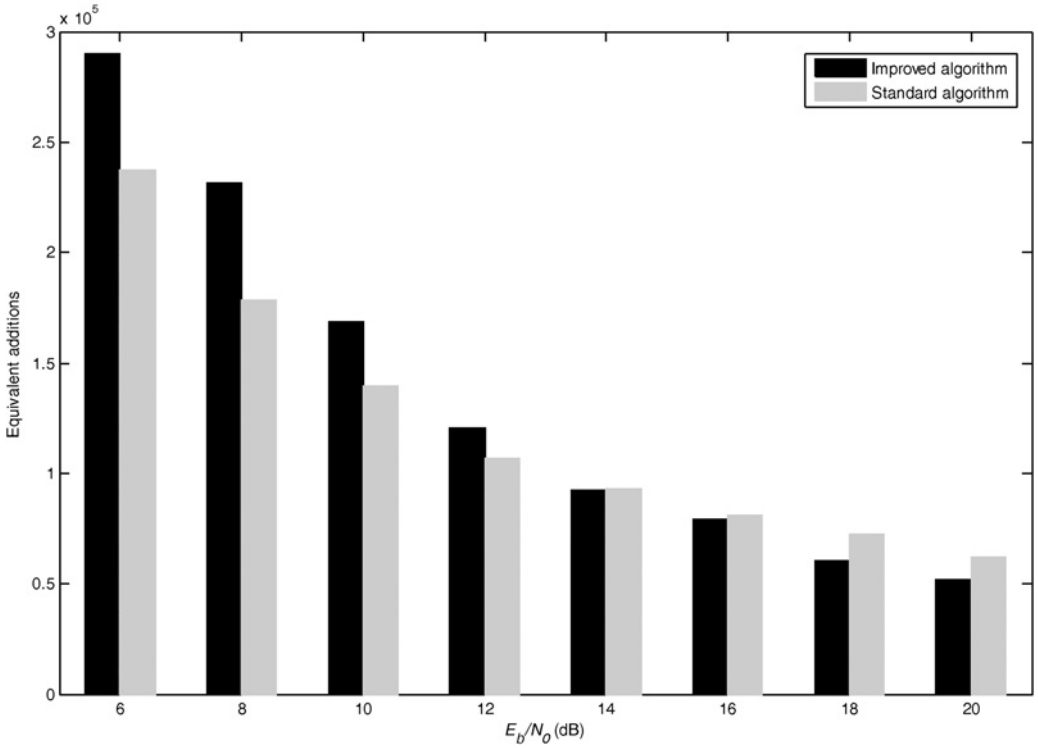

Fig. 6 *Equivalent numbers of addition operations for the joint detection and decoding in JSG-CDMA*

6 Conclusion

In this paper, the joint detection and decoding in JSG-CDMA is researched. The syndrome computation of the message passing on the JSG is investigated, consequently an improved algorithm is proposed. The EXIT chart is analysed for standard and improved algorithms, indicating that improved algorithm can eliminate MAI more effectively. Simulation results show that compared with standard algorithm, improved algorithm has several advantages such as owing a better BER performance, less iteration numbers and a more uniform user experience. In terms of the receiver complexity, improved algorithm needs more computational operations than standard algorithm in the low E_b/N_0 region, but reduces the complexity in the high E_b/N_0 region thanks to the decreased number of iterations. Overall, improved algorithm for the JSG-CDMA leads to better performance and faster convergence rate.

7 Acknowledgments

The funding leading to this work was from the 5G innovation centre of University of Surrey, the United Kingdom Engineering and Physical Science Research Council (EPSRC) under grant number EP/J017655/1, the National Natural Science Foundation of China (NSFC) under grant 61372098 and the State Key Laboratory of Astronautic Dynamics open fund (2013ADL-DW0401).

8 References

1 Fantacci, R., Chiti, F., Marabissi, D., *et al.*: 'Perspectives for present and future CDMA-based communications systems', *IEEE Commun. Mag.*, 2005, **43**, (2), pp. 0163–6804
2 Junshan, Z., Konstantopoulos, T.: 'Multiple-access interference processes are self-similar in multimedia CDMA cellular networks', *IEEE Trans. Inf. Theory*, 2005, **51**, (3), pp. 1024–1038
3 Liu, P., Zhengyuan, X.: 'Blind MMSE-constrained multiuser detection', *IEEE Trans. Veh. Technol.*, 2008, **57**, (1), pp. 608–615
4 Haghighat, P., Ghrayeb, A.: 'Trickle-based interference cancellation schemes for CDMA systems', *IEEE Trans. Wirel. Commun.*, 2009, **8**, (1), pp. 13–17
5 Tsan-Ming, W., Tsung-Hua, T.: 'Successive interference cancelers for multimedia multicode DS-CDMA systems over frequency-selective fading channels', *IEEE Trans. Inf. Theory*, 2009, **55**, (5), pp. 2260–2282
6 Nguyen, H.H., Shwedyk, E.: 'A new construction of signature waveforms for synchronous CDMA systems', *IEEE Trans. Broadcasting*, 2005, **51**, (4), pp. 520–529
7 Vanhaverbeke, F., Moeneclaey, M.: 'Sum capacity of equal-power users in overloaded channels', *IEEE Trans. Commun.*, 2005, **53**, (2), pp. 228–233
8 Wathan, F.P., Hoshyar, R., Tafazolli, R.: 'Iterated SISO MUD for synchronous un-coded CDMA systems over AWGN channel: performance evaluation in overloaded condition'. Int. Symp. on Communications and Information Technologies, 2007, pp. 397–402
9 Wathan, F.P., Hoshyar, R., Tafazolli, R.: 'Dynamic grouped chip-level iterated multiuser detection based on Gaussian forcing technique', *IEEE Commun. Lett.*, 2008, **12**, (3), pp. 167–169
10 Hoshyar, R., Wathan, F.P., Tafazolli, R.: 'Novel low-density signature for synchronous CDMA systems over AWGN channel', *IEEE Trans. Signal Process.*, 2008, **56**, (4), pp. 1616–1626
11 Arora, S., Daskalakis, C., Steurer, D.: 'Message-passing algorithms and improved LP decoding', *IEEE Trans. Inf. Theory*, 2012, **58**, (12), pp. 7260–7271
12 Yong, L., Wensheng, N.: 'High throughput LDPC decoder on GPU', *IEEE Commun. Lett.*, 2014, **18**, (2), pp. 344–347
13 Wen, L., Su, M.: 'Joint sparse graph over GF(q) for code division multiple access systems', *IET Commun.*, 2015, **9**, (5), pp. 707–718
14 Koetter, R., Singer, A.C., Tuchler, M.: 'Turbo equalization', *IEEE Signal Process. Mag.*, 2004, **21**, (1), pp. 67–80
15 Sharon, E., Litsyn, S., Goldberger, J.: 'Efficient serial message-passing schedules for LDPC decoding', *IEEE Trans. Inf. Theory*, 2007, **53**, (11), pp. 4076–4091
16 Tiejun, L., Feichi, L.: 'Graph-based low complexity detection algorithms in multiple-input-multiple-out systems: an edge selection approach', *IET Commun.*, 2013, **7**, (12), pp. 1202–1210
17 Yoo, H., Lee, Y., Park, I.C.: 'Area-efficient syndrome calculation for strong BCH decoding', *Electron. Lett.*, 2011, **47**, (2), pp. 107–108
18 Lechner, G., Pacher, C.: 'Estimating channel parameters from the syndrome of a linear code', *IEEE Commun. Lett.*, 2013, **17**, (11), pp. 2148–2151
19 Ardakani, M., Chan, T.H., Kschischang, F.R.: 'EXIT-chart properties of the highest-rate LDPC code with desired convergence behavior', *IEEE Commun. Lett.*, 2005, **9**, (1), pp. 52–54
20 Arnone, L.J., Moreira, J.C., Farrell, P.G.: 'Field programmable gate arrays implementations of low complexity soft-input soft-output low-density parity-check decoders', *IET Commun.*, 2012, **6**, (12), pp. 1670–1675
21 Guojun, H., Yong, L.G., Lingjun, K.: 'Construction of irregular QC-LDPC codes via masking with ACE optimization', *IEEE Commun. Lett.*, 2014, **18**, (2), pp. 348–351
22 Ioannis, A.C., Miguel, R.D.R., Ian, J.W., *et al.*: 'Comparison of convolutional and turbo coding for broadband FWA systems', *IEEE Trans. Broadcasting*, 2007, **53**, (2), pp. 494–503